NAVAL POSTGRADUATE SCHOOL

MONTEREY, CALIFORNIA

THESIS

MODELING THE EFFECTS OF TRANSBASIN NONLINEAR INTERNAL WAVES THROUGH THE SOUTH CHINA SEA BASIN

by

Joseph J. Ceschini

June 2013

Thesis Advisor: Ching-Sang Chiu
Second Reader: John Joseph

Approved for public release; distribution is unlimited

THIS PAGE INTENTIONALLY LEFT BLANK

REPORT DOCUMENTATION PAGE

Form Approved OMB No. 0704-0188

1. AGENCY USE ONLY *(Leave blank)*	**2. REPORT DATE** June 2013	**3. REPORT TYPE AND DATES COVERED** Master's Thesis

4. TITLE AND SUBTITLE
MODELING THE EFFECTS OF TRANSBASIN NONLINEAR INTERNAL WAVES THROUGH THE SOUTH CHINA SEA BASIN

5. FUNDING NUMBERS

6. AUTHOR(S) Joseph J. Ceschini

7. PERFORMING ORGANIZATION NAME(S) AND ADDRESS(ES)
Naval Postgraduate School
Monterey, CA 93943-5000

8. PERFORMING ORGANIZATION REPORT NUMBER

9. SPONSORING /MONITORING AGENCY NAME(S) AND ADDRESS(ES)
N/A

10. SPONSORING/MONITORING AGENCY REPORT NUMBER

11. SUPPLEMENTARY NOTES The views expressed in this thesis are those of the author and do not reflect the official policy or position of the Department of Defense or the U.S. government. IRB Protocol number ____N/A____.

12a. DISTRIBUTION / AVAILABILITY STATEMENT
Approved for public release; distribution is unlimited

12b. DISTRIBUTION CODE
A

13. ABSTRACT (maximum 200 words)

The objective of this research is to model and study the effects of transbasin internal waves on low-frequency signal transmission through the South China Sea (SCS) basin. Specifically, the fluctuations in the multipath arrival structure of a 400-Hz acoustic pulse transmitted through a distance of 167-km in the SCS basin in the presence of an internal ocean soliton was modeled and examined. The modeling entailed the integration of a raytracing program with an eigenray search and arrival-structure calculation program, and the use of measured bathymetry and inferred bottom-loss characteristics from previous research. A range-dependent perturbation was added to a range-independent background sound-speed profile to model the varying sound-speed field as the nonlinear ocean internal soliton propagates along the transmission path. All cases studied, each simulating a soliton at a different location, had six distinct acoustic arrivals that suffered from large-amplitude fluctuations (~ 10 dB). The factors that affect the amplitude of the arrivals are changes: in the number of bottom interaction, in ray tube spreading, phase interference and in the number of eigenrays making up an arrival. The results also show that the closer the soliton to the receiver, the less impact the soliton has on the arrival structure.

14. SUBJECT TERMS South China Sea, soliton, nonlinear internal wave, computational acoustics model	**15. NUMBER OF PAGES** 51
	16. PRICE CODE

17. SECURITY CLASSIFICATION OF REPORT	**18. SECURITY CLASSIFICATION OF THIS PAGE**	**19. SECURITY CLASSIFICATION OF ABSTRACT**	**20. LIMITATION OF ABSTRACT**
Unclassified	Unclassified	Unclassified	UU

NSN 7540-01-280-5500

Standard Form 298 (Rev. 2-89)
Prescribed by ANSI Std. 239-18

THIS PAGE INTENTIONALLY LEFT BLANK

Approved for public release; distribution is unlimited

MODELING THE EFFECTS OF TRANSBASIN NONLINEAR INTERNAL WAVES THROUGH THE SOUTH CHINA SEA BASIN

Joseph J. Ceschini
Lieutenant, United States Navy
B.S., Pennsylvania State University, 2004

Submitted in partial fulfillment of the
requirements for the degree of

MASTER OF SCIENCE IN METEOROLOGY AND PHYSICAL OCEANOGRAPHY

from the

NAVAL POSTGRADUATE SCHOOL
June 2013

Author: Joseph J. Ceschini

Approved by: Ching-Sang Chiu
Thesis Advisor

John Joseph
Second Reader

Peter Chu
Chair, Department of Oceanography

THIS PAGE INTENTIONALLY LEFT BLANK

ABSTRACT

The objective of this research is to model and study the effects of transbasin internal waves on low-frequency signal transmission through the South China Sea (SCS) basin. Specifically, the fluctuations in the multipath arrival structure of a 400-Hz acoustic pulse transmitted through a distance of 167-km in the SCS basin in the presence of an internal ocean soliton was modeled and examined. The modeling entailed the integration of a raytracing program with an eigenray search and arrival-structure calculation program, and the use of measured bathymetry and inferred bottom-loss characteristics from previous research. A range-dependent perturbation was added to a range-independent background sound-speed profile to model the varying sound-speed field as the nonlinear ocean internal soliton propagates along the transmission path. All cases studied, each simulating a soliton at a different location, had six distinct acoustic arrivals that suffered from large-amplitude fluctuations (~ 10 dB). The factors that affect the amplitude of the arrivals are changes: in the number of bottom interaction, in ray tube spreading, phase interference and in the number of eigenrays making up an arrival. The results also show that the closer the soliton to the receiver, the less impact the soliton has on the arrival structure.

THIS PAGE INTENTIONALLY LEFT BLANK

TABLE OF CONTENTS

THIS PAGE INTENTIONALLY LEFT BLANK

LIST OF FIGURES

LIST OF TABLES

THIS PAGE INTENTIONALLY LEFT BLANK

LIST OF ACRONYMS AND ABBREVIATIONS

EOF	Empirical Orthogonal Function
HARPO	Hamiltonian Acoustic Ray-tracing Program for the Ocean
NE	Northeastern
NPS	Naval Postgraduate School
OASIS	Ocean Acoustical Services and Instrumentation Systems
SCS	South China Sea
WISE	Windy Islands Soliton Experiment
WHOI	Woods Hole Oceanographic Institute

THIS PAGE INTENTIONALLY LEFT BLANK

ACKNOWLEDGMENTS

First, I would like to offer deep gratitude to Professor C. S. Chiu. Thank you for your patience and guidance throughout the entire thesis process. Second, I would like to thank Professor John Joseph. Next, I would like to acknowledge Dr. Y. T. Lin, WHOI, for sharing his three-dimensional raytracing MATLAB program. Next, I would like to thank Chris Miller. You have been a sounding board for me during this process and without your help I would still be working on my thesis. Last, but not, least I would like to thank my wife and children. Without your love and support I would not be where I am today.

THIS PAGE INTENTIONALLY LEFT BLANK

I. INTRODUCTION

A. NAVAL IMPORTANCE

The current Defense Strategic Guidance states while the U.S. military will continue to contribute to security globally, we will of necessity rebalance toward the Asia-Pacific region. In order to do this, the Navy must be able to understand the operational environment within the Asia-Pacific region. The South China Sea (SCS) is an area of significant strategic and tactical importance to the Navy. A large portion of the world's commerce travels on the shipping lanes located in the SCS. An accurate model of the phenomenology of sound propagation through the SCS needs to be developed to help maintain tactical superiority. This model will provide valuable information for operational planning and execution in the South China Sea.

B. SOUTH CHINA SEA BACKGROUND

The SCS is the westernmost marginal sea of the Pacific Ocean. The SCS has borders of Straits of Malacca to southwest, the Taiwan Strait to the northeast, and the Luzon Strait to the east. The SCS stretches from Taiwan to Singapore. The bottom consists of a deep basin with depths greater than 4,000 m and two extended continental shelves, one to the north and one to the south.

The SCS has environmental variability on numerous scales ranging from super-tidal to inter-annual. These include intrusion of the Kuroshio Current, variable wind forcing, and large amplitude internal waves. The seasonal variability is governed by the monsoons. The variable wind forcing is due to the tropical monsoon climate. The Kuroshio Current is the western boundary current of the northwestern Pacific Ocean. It has been observed to enter via the Luzon Strait and then have widely variable behavior. Possible scenarios include simply exiting, bifurcation, or forming a warm mesoscale eddy that can propagate across the SCS (Ramp et al. 2004). The large amplitude internal waves are generated by the interaction of the sharp change in topography and the strong

tidal currents near the Luzon Strait. The largest ever observed internal waves occur in this region (Hsu & Liu 2000). These waves dominate the ocean variability in the northeastern (NE) SCS basin. These non-linear waves can significantly effect the acoustic propagation in the basin.

C. WISE EXPERIMENT

The Windy Islands Soliton Experiment (WISE) was an integrated acoustics and physical oceanography experiment, an international collaboration between the Naval Postgraduate School (NPS), National Taiwan University, National Sun Yet-Sen University, Ocean Acoustical Services and Instrumentation Systems (OASIS), and Woods Hole Oceanographic Institute (WHOI). The experiment took place in the NE SCS and Luzon Strait and lasted one year, April 2005–2006. One of the main goals of WISE was to study the evolution of trans-basin nonlinear internal waves (Ramp et al. 2010). Moorings were placed on the shelf, in the Luzon strait, and the deep basin.

In WISE two acoustic propagation studies were conducted, one on the continental shelf and one in the deep basin. The focus of these was to study the physics, phenomenology, and statistics of sound propagation in the NE SCS. The objective of the basin propagation experiment was to study and characterize the supertidal to seasonal scale impacts of the trans-basin, nonlinear internal waves on long-range transmission loss, and to help monitor the evolution of the trans-basin internal waves in the basin's interior (Miller et al. 2009). This was completed by the use of two deep-water moorings that transmitted and received a 400 Hz signal repeatedly over a one-year period. Modeling of the observed arrival structure is the focus of this thesis. The location of these moorings are shown in Figure 1.

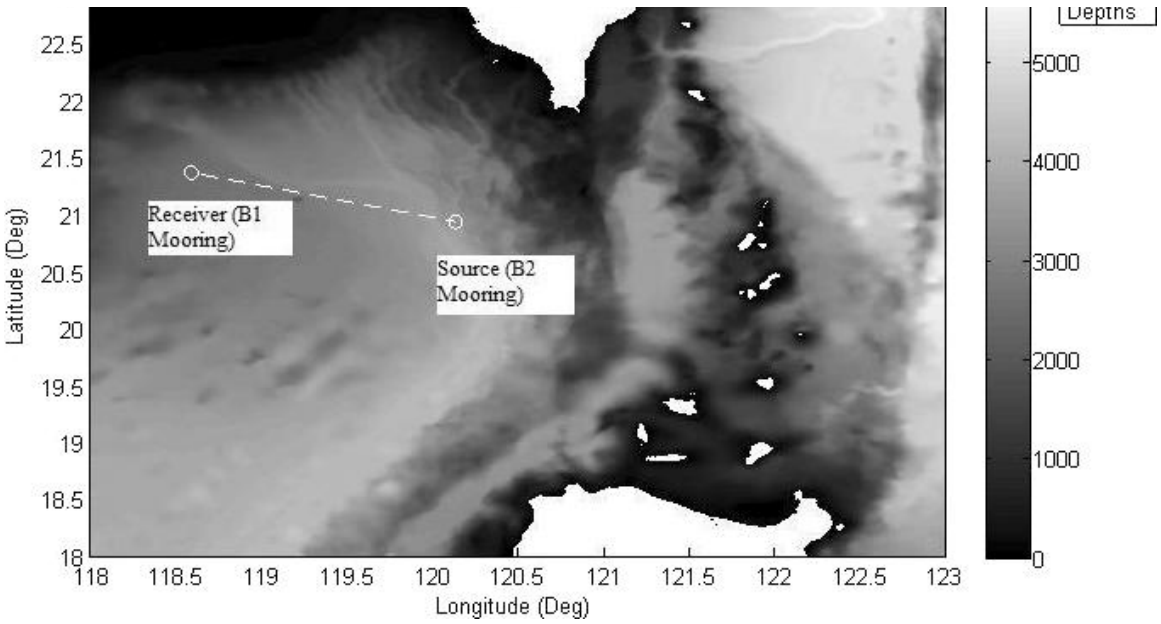

Figure 1. Locations of the source (B2) and receiver (B1) in the SCS superimposed on the bathymetry (From Bernotavicius et al. 2010).

D. OBJECTIVE

The objective of this research is to model and study the effects of the transbasin internal waves on low-frequency signal transmission through the SCS basin. Specifically, the fluctuations in the multipath arrival structure of a 400-Hz acoustic pulse transmitted through a distance of 167-km in the NE SCS basin in the presence an internal ocean soliton. Previous research by Bernotavicius (2010) modeled the background arrival structure in the unperturbed SCS basin using the Hamiltonian Acoustic Ray-tracing Program for the Ocean (HARPO). That research used a silty clay type bottom. A bottom attenuation rate of .486 dB/km/Hz, a bottom density of 1.24 kg/km^3 and a bottom sound speed of 1,521 m/s were used. That accurately modeled the mean arrival structure for the SCS basin. An initial launch angle angular resolution of .005 degrees was used. That resolution or finer was able to capture all the eigenrays (Bernotavicius et al. 2010). This research will study the fluctuations in the arrival structure caused by the nonlinear ocean solitons.

E. APPROACH

The approach of this thesis was to develop a numerical model of a 400 Hz signal transmission through the SCS in the presence of a trans-basin internal soliton and then examine and contrast the modeled arrival structures at the receiver. The model is based on ray theory, and entails the integration of a raytracing model and an eigenray ray search and arrival structure simulation code. The model permits the study of the physics and phenomenology of sound propagation though the SCS trans-basin nonlinear internal waves. A modeled range dependent sound speed profile, measured bathymetry and inferred bottom-loss characteristics from previous research were used.

F. THESIS OUTLINE

The rest of this thesis contains three chapters. Chapter II describes the ray trace model, the eigenray search and arrival structure simulation model, and the methodology used to integrate the ray trace model with the eigenray search arrival structure simulation. Chapter III describes the results of the five cases studied. A summary of results and conclusions are given in Chapter IV.

II. METHODOLOGY

A. ACOUSTIC MODEL

1. Ray Trace Theory

Modeling of sound propagation through the ocean requires solving the governing spherical wave equation:

$$\nabla^2 p - \frac{1}{c(\vec{r})}\frac{\partial^2 p}{\partial t^2} = 0 \tag{2.1}$$

subject to the appropriate surface and bottom boundary conditions. Here *p* is the sound pressure, *c* is sound speed, *t* is time, and $\vec{r}$ is a position vector (Medwin, 2005). The assumption is made in ray acoustics that variation in sound speed is gradual over a small number of acoustic wavelengths. It is also assumes that solutions of the equation take the following form:

$$p(\vec{r},t) = A(\vec{r})\exp\left(i\left[2\pi ft - k_0 W(\vec{r})\right]\right) \tag{2.2}$$

where $k_0 = \frac{2\pi f}{c_0}$ is the reference wave number, c_0 is the reference sound speed, f is the acoustic frequency, and $W(\vec{r})$ is the eikonal when multiplied by k_0 gives the phase component of the solution. Equation 2.2 is substituted into Equation 2.1 to yield the eikonal and transport equations in Equation 2.3. The eikonal yields the ray equations and the ray paths while the transport equation governs the ray amplitude. The phase is determined by integrating ekional along the ray path. This results in the phase equaling $2\pi f\tau$ where τ is the ray travel time. The ratio of a reference sound speed to sound speed $\left(c_0 / c(\vec{r})\right)$ is the quantity *n*, called the index of refraction and *s* is the distance along the ray path.

$$\text{Eikonal Equation: } \left|\nabla W(\vec{r})\right|^2 = n^2(\vec{r})$$
$$\text{Transport Equation: } 2\nabla \mathrm{A}(\vec{r})\cdot\nabla W(\vec{r}) + A(\vec{r})\nabla^2 W(\vec{r}) = 0 \qquad (2.3)$$
$$\text{Ray Equation: } \frac{d}{ds}\left(n(\vec{r})\frac{d\vec{r}}{ds}\right) = \nabla n(\vec{r})$$

Ray theory assumes that diffractive leakage is small and the change in amplitude occurs slowly. The transport equation implies that power must be conserved along a ray tube. A full derivation of these equations can be found in a reference such as Ziomek (1995).

A three-dimensional ray trace model developed by Y. T. Lin (2012, personal communication) at WHOI was used for this thesis. This model is MATLAB based and is intended to replace the HARPO model used in previous research. HARPO is a FORTRAN based model that can only run on obsolete computer systems. The model was reduced to a two dimensional model. An initial launch angle angular resolution of .005 degrees was used in the raytracing. An initial launch angle angular aperture of -20 to 20 degrees was used. This captures all eigenrays that significantly contribute and minimizes computational requirements (Bernotavicius et al. 2010).

2. Eigenray Determination

To model the multipath acoustic arrival structure, it is necessary to identify the acoustic paths connecting the source to the receiver, i.e., eigenrays. The eigenray search and arrival structure simulation MATLAB code of Chiu (1994) was integrated with output of the raytrace model to calculate the eigenray parameters and arrival structure. This code determines the depth difference at the receiver range between the receiver and the ray as a function of initial launch angle. Locating the zeros on this curve allows for the eigenray parameters to be interpolated accurately. No rays are retraced while determining the eigenrays. For the plotting of eigenrays, those rays located nearest to the eigenrays are used. This code accurately interpolates using higher order polynomial fitting for the eigenray parameters including amplitude, phase, and phase front arrival time.

Once the eigenray parameters are determined the arrival structure can be generated using Equation 2.4. A model pulse is created to match the energy and shape of the source signal complex envelop used in WISE. Given this pulse complex envelop and the eigenray parameters the arrival structure can be calculated as:

$$\tilde{r}(t) = \sum_{eigenrays} \tilde{s}(t - t_n) a_n e^{-i(2\pi f_c t_n + \varphi_n)} \tag{2.4}$$

where $\tilde{r}$ represents the complex envelop at the receiver and $\tilde{s}$ represents the complex envelop at the source. A more detailed discussion of this approximation can be found in Hager (2008).

B. MODEL INPUT

1. Model Domain

In the model, the sound source and receiver were located at the B2 and B1 locations shown in Figure 1, placed 167 km apart and located at a depth of 800 m. This was done to model the sound source at the B2 mooring and the receiver at the B1 mooring. A signal center frequency of 400 Hz was used. A bottom attenuation rate of .486 dB/km/Hz, a bottom density of 1.24 kg/km^3, and a sediment sound speed of 1.521 km/s were used. These bottom parameters best represent the bottom loss characteristics of the NE SCS (Bernotavicius et al. 2010). An rms surface roughness of zero was chosen to represent a smooth sea surface. This was done to remove any losses due to surface roughness suffered by the rays. Bathymetry was obtained from high resolution transects of the Luzon Strait (Liu et al. 1998). This data was smoothed using a cubic spline to give a continuous bathymetry for raytracing.

2. Sound Speed

For this research a two dimensional range dependent sound speed profile was used. The modeled perturbed sound speed profile consists of a background unperturbed profile $\overline{c}(z)$ that is range independent and a perturbation $\delta c(r,z)$, which depends on range r and depth z.

$$c(r,z) = \bar{c}(z) + \delta c(r,z) \tag{2.5}$$

The sound speed profile was determined using the Medwin sound speed equation (Medwin, 1975) applying temperature salinity and depth data. The data includes a three-month time series of temperature with a sampling rate of one minute, at the B1 mooring. This mooring provided temperatures at the following nine depths in meters: 125, 173, 375, 500, 755, 1000, 1385, 1884, and 2438. The data also includes the mean salinity profile from the CTD casts conducted during the WISE experiment. The minimum value of sound speed for each depth was used to represent the unperturbed sound speed profile. This is due to the fact that the transbasin solitons are depression internal waves and hence they would only lead to sound speed increases. For depths less than 125 meters, the sound speed gradient at 125 meters was extrapolated to the surface. For depths below 2438 meters, the sound speed was extrapolated using a constant sound speed gradient of $.016\ \mathrm{s}^{-1}$.

3. Sound Speed Perturbation

The sound speed perturbations were assumed to have a separable form, consisting of a vertical component and a horizontal component. The equation for the perturbation is therefore.

$$\delta c(r,z) = \alpha(z) \bullet \beta(r) \tag{2.6}$$

To determine the vertical component of the sound speed perturbations, an Empirical Orthogonal Function (EOF) analysis was performed on the sound speed time series calculated from the temperature, salinity and depth information. EOF analysis is a common tool used to determine the dominant structure of a data set. EOF analysis decomposes the data into orthogonal functions. The resulting orthogonal functions will be rank ordered by variance. The first orthogonal function contains the most variance. The EOF analysis conducted on the sound speed time series showed that the first orthogonal function contained 95 percent of the variance. The remaining five percent of the variance was spread among the remaining eight orthogonal functions. The first

orthogonal function was chosen to represent the vertical structure of a soliton. A more detailed description of this method of data analysis can be found in Wilks (2006). The vertical component is shown in Figure 2. This was obtained by a cubic spline fit through the points of the first orthogonal function and zero at the surface and a depth of 4,000 m. The vertical structure was normalized to have a maximum value of unity. The depth of maximum influence for the modeled soliton is 91 m.

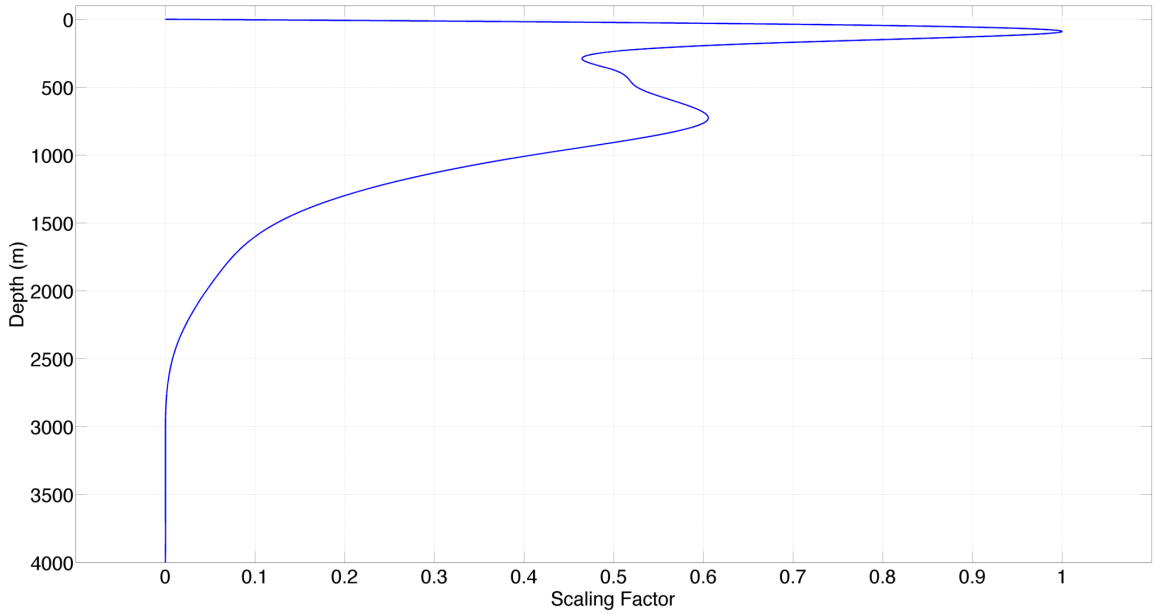

Figure 2. Sound speed perturbation vertical structure derived from EOF analysis of sound speed profile time series.

The modeled horizontal component is shown in the Equation 2.7, which is adopted from (Chiu et al. 2004):

$$\beta(r) = \delta \ \mathrm{sech}^2\left(2\pi \frac{r - r_o}{\Delta}\right)$$

$$\delta = 15 \ \frac{m}{s} \qquad (2.7)$$

$$\Delta = 11{,}520 \ \mathrm{m}$$

$$r_0 = \ \text{Center location}$$

where δ is the soliton amplitude, Δ is the soliton width, and r_0 is the soliton center location. The values used for the model soliton width and amplitude were taken from the WISE dataset. The soliton width was shifted from time to space using a soliton phase speed of 1.25 m/s (Ramp et al. 2004). How closely this structure matches observed data is shown in Figure 3. For this research, a soliton was placed in five different locations 40, 60, 80, 120, and 160 km from the source. This is to represent a soliton transiting the basin. The vertical and horizontal components are combined to represent the sound speed perturbation that is shown in Figure 4.

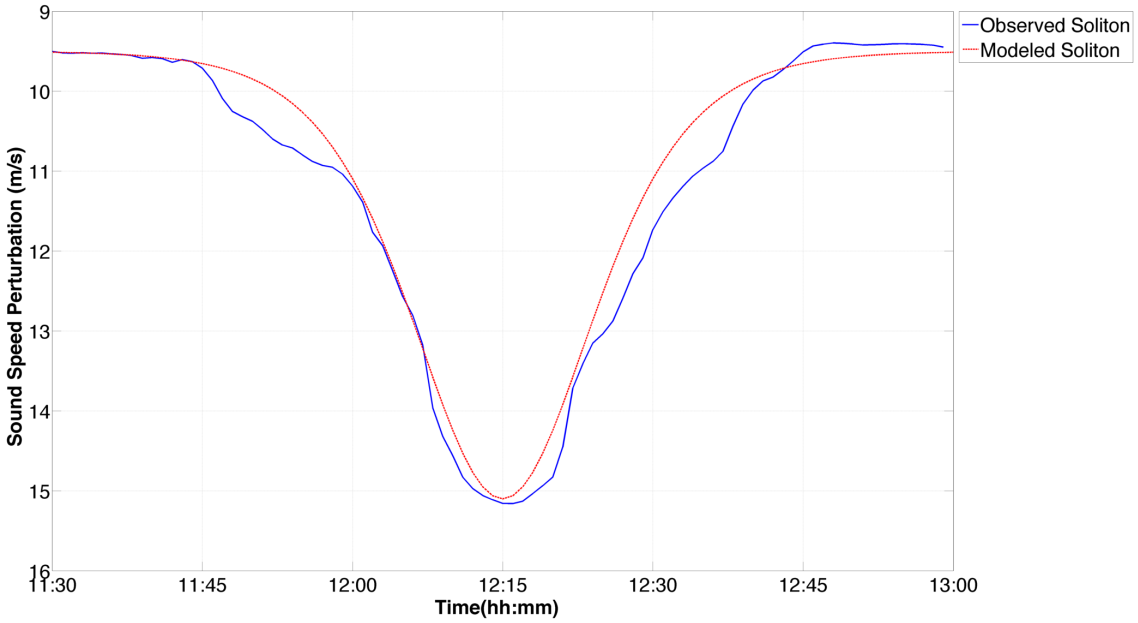

Figure 3. The horizontal structure of the sound speed perturbation. Both the modeled (red) and observed (blue) are shown.

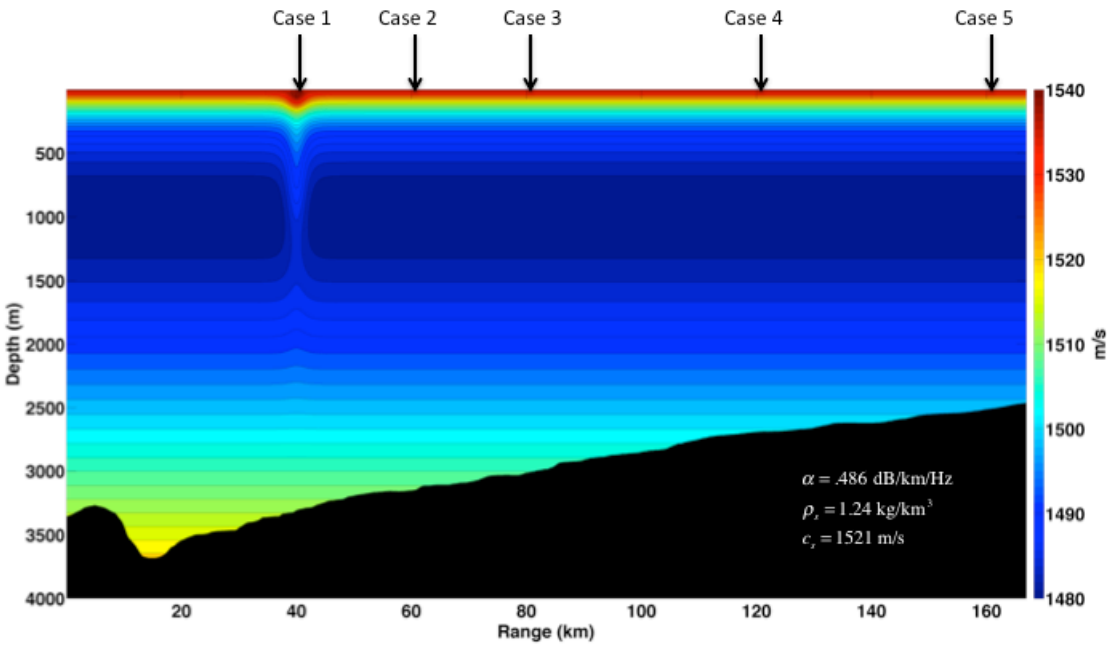

Figure 4. Contour plot of the modeled sound speed with an internal soliton located at 40 km overlaying the bathymetry. The bottom attenuation rate, bottom density and bottom sound speed are also displayed.

For this research a soliton was placed at five different locations in the model domain. A model run was also conducted with no soliton; this will be referred to as the unperturbed case. The collection of the five cases is meant to represent a soliton transiting across the NE SCS basin. The location of the soliton center in each case is shown in Table 1.

Case #	Location of Soliton Center
1	40 km
2	60 km
3	80 km
4	120 km
5	160 km

Table 1. Center location of the ocean internal soliton for each case.

THIS PAGE INTENTIONALLY LEFT BLANK

III. RESULTS

A. OVERVIEW

Consistently, each perturbation case and the unperturbed case has six separate arrivals. Their arrival times are approximately constant at: 112.8s, 112.9s, 113.1s, 113.3s, 113.5s, and 113.7s, respectively. A plot of the modeled sound pressure (in dB re $1\mu Pa$) versus travel time for each of the five cases and the unperturbed case is shown in Figure 5. Although the arrival times are rather robust, large fluctuations in amplitude for each arrival are present. The factors that affect the amplitude for each of the arrivals are: bottom interaction, change in ray tube spreading, phase interference and an increase/decrease in the number of eigenrays making up an arrival. These factors will be illustrated in the subsequent sections. In two of the cases the second arrival diminishes greatly. Each arrival for each perturbation case is slightly ahead of the corresponding arrival in the unperturbed case. This is due to the transbasin soliton being a depression wave that leads to an increase in sound speed.

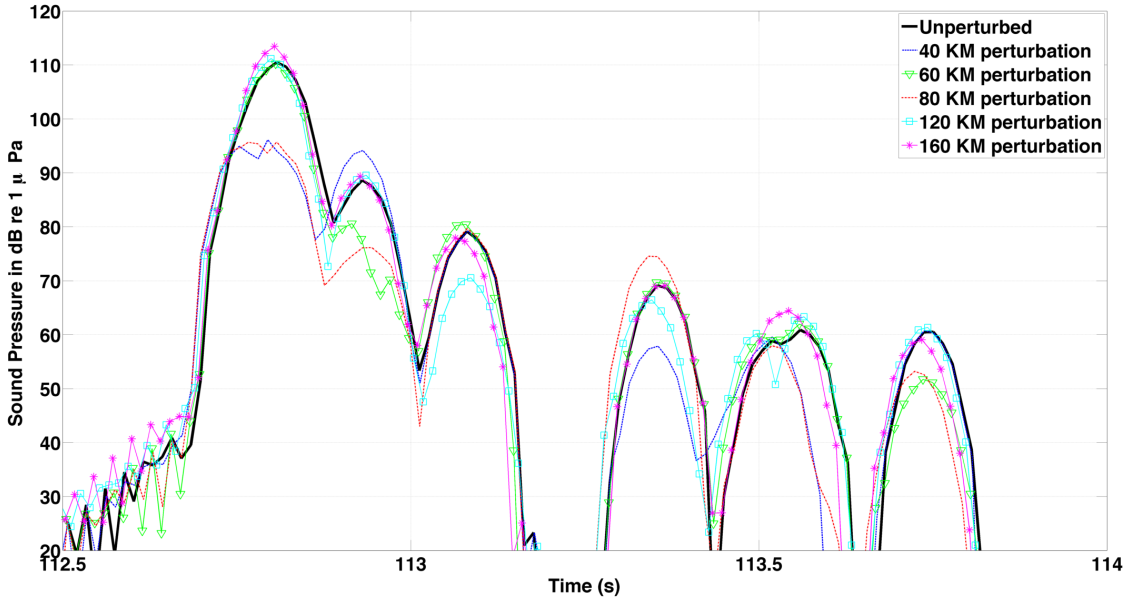

Figure 5. Acoustic arrival structure (receive level versus travel time) for each case and the unperturbed case.

For some arrivals in the perturbed cases the associated number of eigenrays changes. This is associated with micropathing caused by the relatively strong gradients. In addition the sharp sound speed gradient in the perturbed cases, the locations of bottom interactions can deviate slightly and thus the same group of rays can experience different bathymetry gradients. An example of the existence of micropathing can be seen in Figure 6. Where the curve of arrival depth difference (i.e., arrival depth at the receiver range minus the receiver depth) versus the initial launch angle of rays is smooth, near a low initial launch angle, no micropathing exists. As the initial launch angle increases and the depth difference versus initial launch angle curve sharply changes micropathing begins to develop. Note that the zero crossings of this curve define the initial launch angle of all the eigenrays. The remainder of this chapter will explore the physics and phenomenology of the amplitude changes for each case.

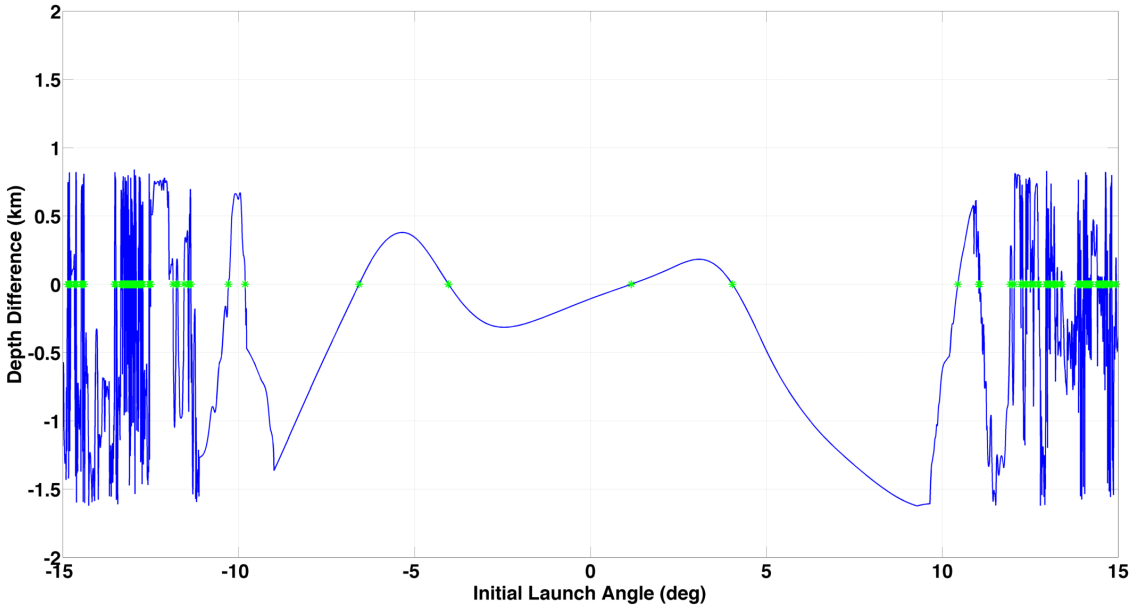

Figure 6. Arrival depth versus initial launch angle. The depth difference is the deviation from the receiver depth. The zeros crossings are the initial launch angles of the eigenrays (shown as green stars).

B. CASE 1

For Case 1 the soliton is placed at 40 km from the source. A plot of the acoustic arrival structure for this case is shown in Figure 7. The first and fourth arrivals have a sound pressure lower than the unperturbed case. The second arrival for case 1 has a higher level than the unperturbed case. The third, fifth, and sixth arrivals are roughly the same.

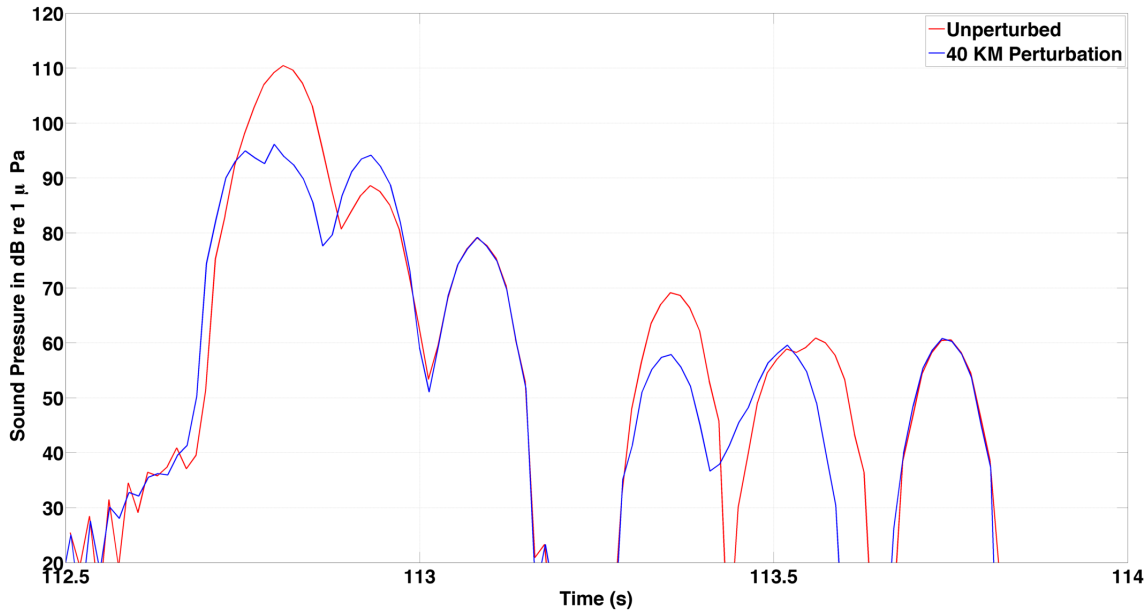

Figure 7. Acoustic arrival structure (receive level versus travel time) for Case 1 (blue) and for the unperturbed case (red).

The ray paths of the eigenrays for the first, second and fourth arrivals are shown in Figure 8. Case 1 is in blue, and the unperturbed case is in red. In the first arrival, a shift in the initial launch angles is seen. For the second arrival, the soliton causes more eigenrays to form, leading to a higher receive level. Case 1 has four eigenrays while the unperturbed case only has two. The fourth arrival shows that the eigenrays for the perturbed case have an additional bottom interaction located around 20 kilometers from the source that the unperturbed case does not show. This is highlighted with a black circle in Figure 8.

Figure 9 is a plot of ray tube spreading loss versus initial launch angle for Case 1 and the unperturbed case. The discrete symbols represent the eigenrays. A shift in the structure of this plot can clearly be seen. The first arrival has increased raytube spreading loss for several of the eigenrays in Case 1. This is highlighted with a black circle in Figure 9.

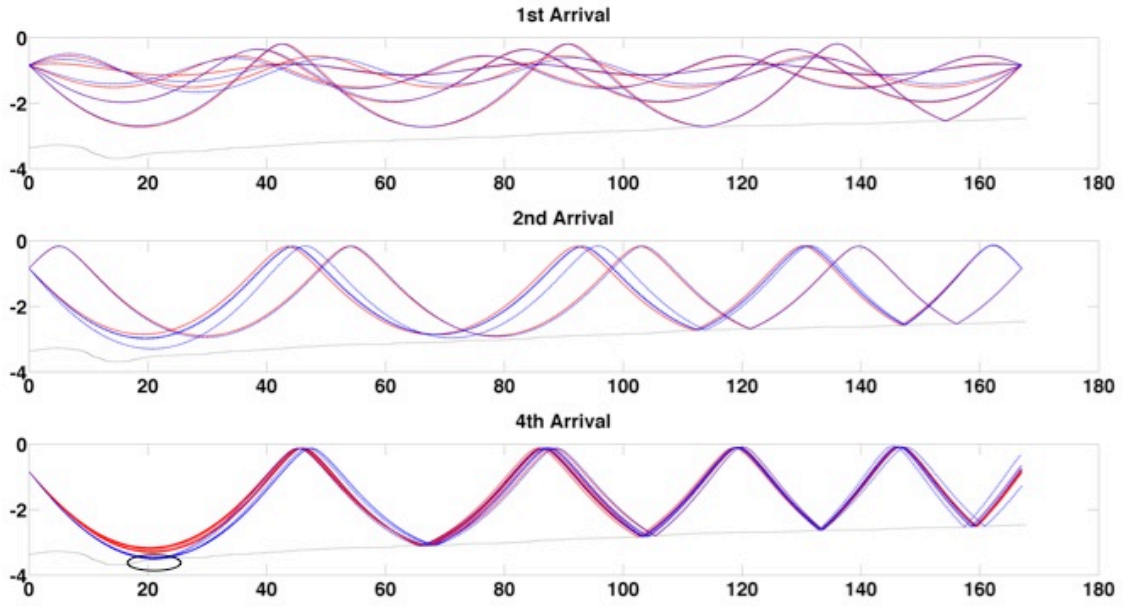

Figure 8. The eigenrays for the 1st, 2nd, and 4th arrivals for Case 1 (blue) and for the unperturbed case (red). Additional bottom interactions for 4th arrival of Case 1 are highlighted in the black circle.

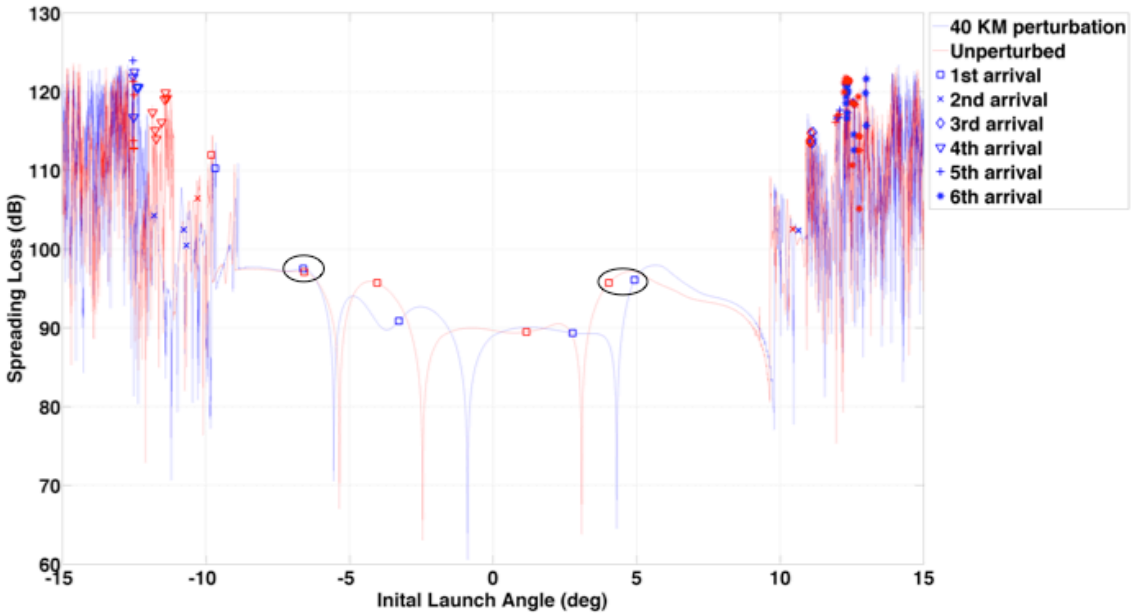

Figure 9. Raytube spreading loss versus initial launch angle (solid lines) for Case 1 (blue) and for the unperturbed case (red). Discrete symbols denote the eigenrays. Increased spreading loss for the 1st arrival of Case 1 is highlighted in the black circles.

A plot of the number of bottom bounces versus initial launch angle is shown in Figure 10. Case 1 is in blue and the unperturbed case is in red. The fourth arrival for Case 1 contains several eigenrays with 5 bottom bounces while the same arrival for unperturbed case has only 4 bottom bounces. This is shown with a black circle in Figure 10. This increase in bottom interactions leads to an increase bottom loss for the fourth arrival seen in Figure 11.

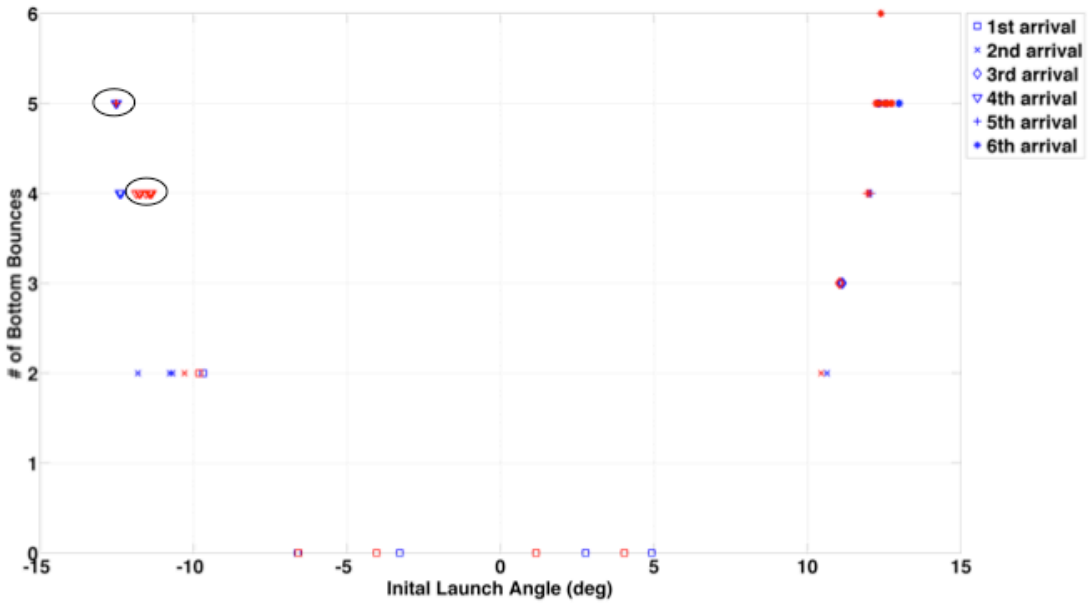

Figure 10. Number of bottom bounces versus initial launch angle for Case 1 (blue) and for the unperturbed case (red). Additional bottom bounces for the 4th arrival of Case1 are highlighted with black circles.

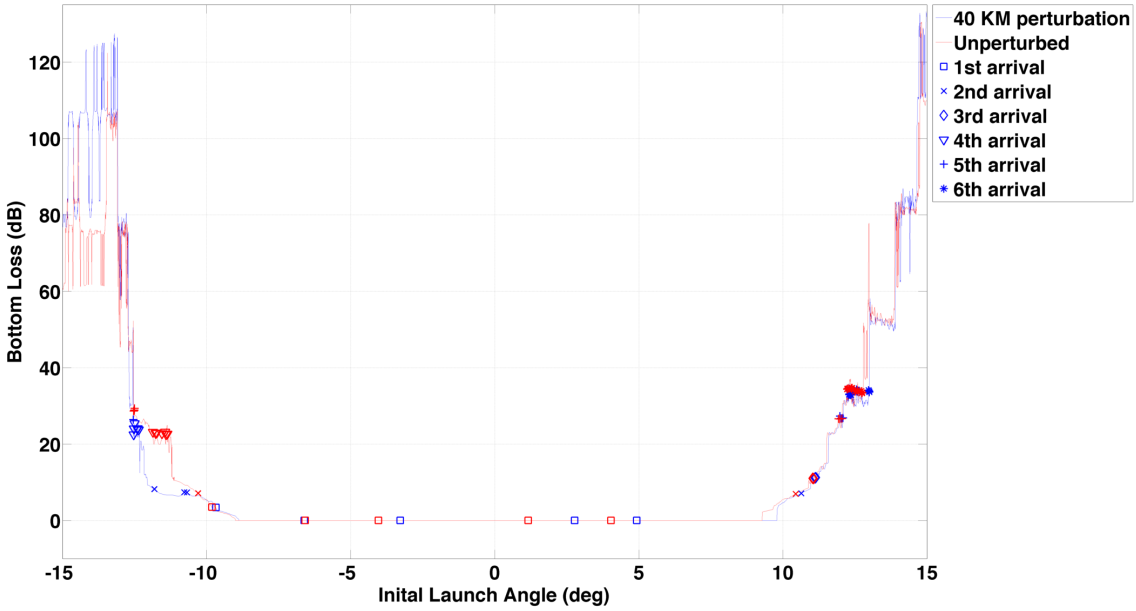

Figure 11. Bottom loss versus initial launch angle (solid lines) for Case 1 (blue) and for the unperturbed case (red). Discrete symbols denote eigenrays.

C. CASE 2

For Case 2, the soliton is placed at 60 km from the source. A plot of the acoustic arrival structure for this case is shown in Figure 12. The second and sixth arrivals are roughly 10 dB lower than the unperturbed case. The first, third, fourth, and fifth arrivals are all similar to the unperturbed case.

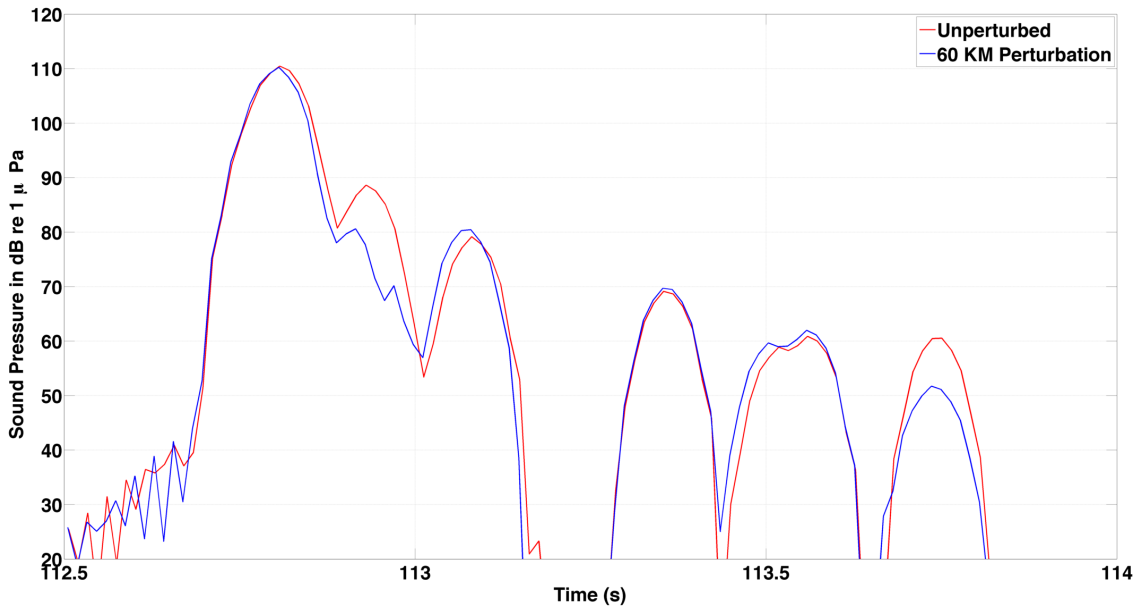

Figure 12. Acoustic arrival structure (receive level versus travel time) for Case 2 (blue) and for the unperturbed case (red).

The eigenrays for the second and sixth arrivals for Case 2 are shown in Figure 13. Case 2 is in blue and the unperturbed case in red. The second arrival for Case 2 and the unperturbed case have only two eigenrays. These two rays for Case 2 are more out of phase then the rays of unperturbed case and therefore have destructive interference for this arrival. The sixth arrival for Case 2 consists of 13 eigenrays while the same arrival for the unperturbed case has 15 eigenrays. This difference in the number of eigenrays combined with the phase interference explains the lower sound pressure.

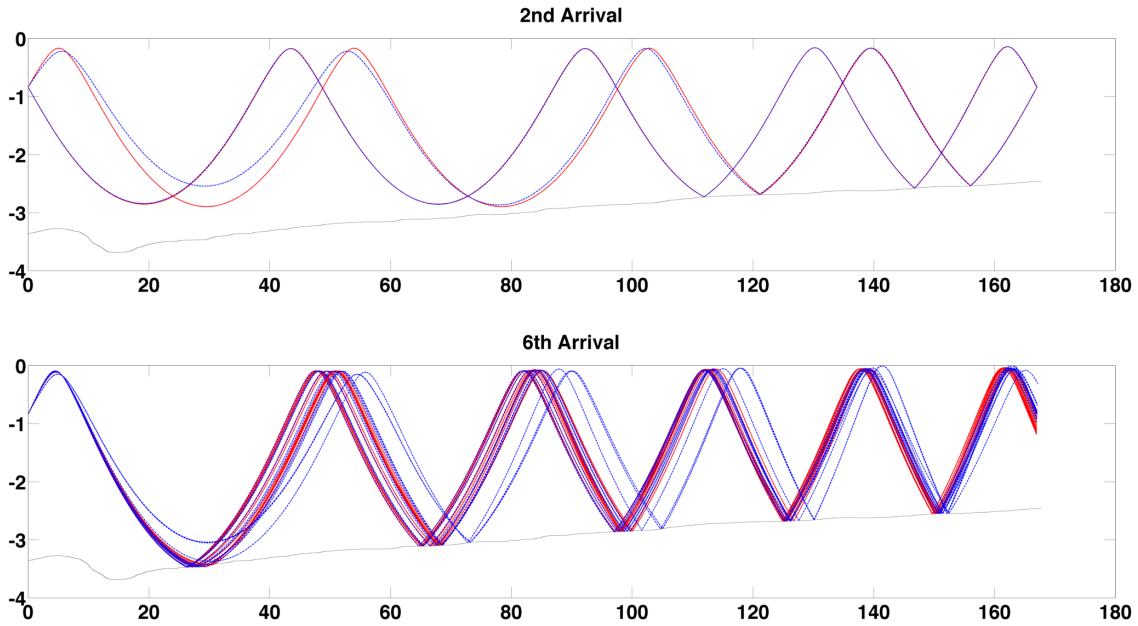

Figure 13. The eigenrays for the 2nd and 6th arrivals for Case 2 (blue) and for the unperturbed case (red).

A plot of ray tube spreading loss versus initial launch angle for Case 3 and for the unperturbed case is shown in Figure 14. A plot of the corresponding bottom loss versus initial launch angle is shown in Figure 15. The second arrival for Case 3 and the unperturbed case have similar values for both ray tube spreading loss and bottom loss. This is shown with blacks circles in Figure 14 and 15. This indicates that destructive interference caused by the two rays being more out of phase is the cause of the decreased sound pressure for the second arrival of Case 3.

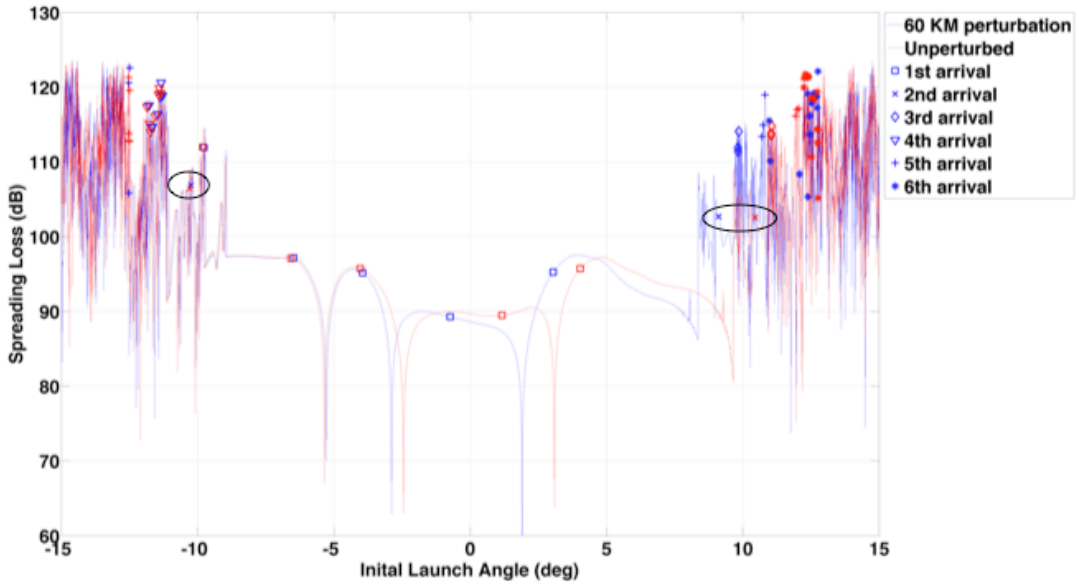

Figure 14. Raytube spreading loss versus initial launch angle (solid lines) for Case 2 (blue) and for the unperturbed case (red). Discrete symbols denote eigenrays. Black circles highlight similar values for 2nd arrival for Case 2 and the unperturbed case.

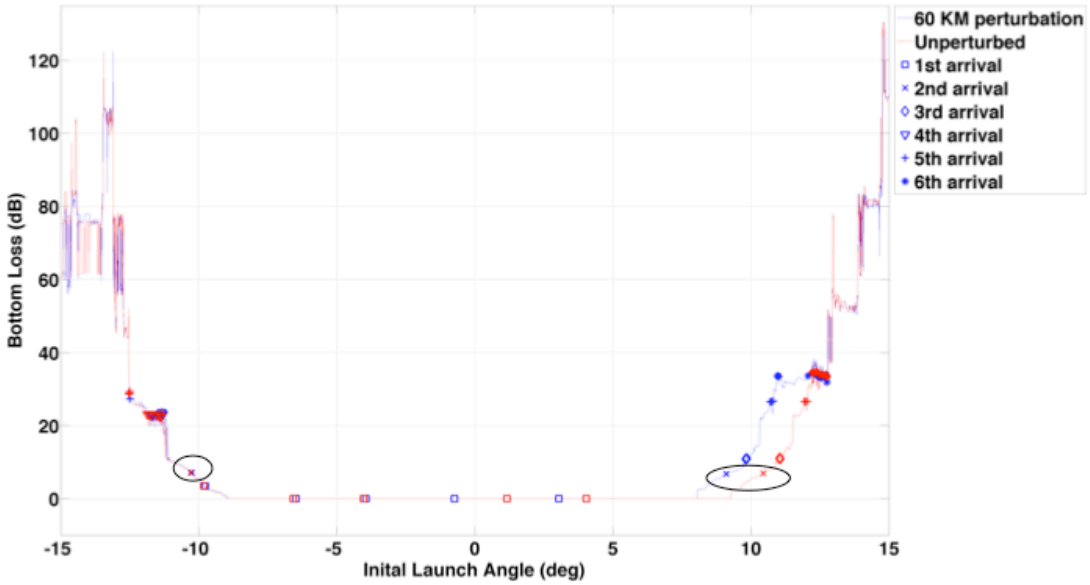

Figure 15. Bottom loss versus initial launch angle (solid lines) for Case 2 (blue) and for the unperturbed case (red). Discrete symbols denote eigenrays. Black circles highlight similar values for 2nd arrival for Case 2 and the unperturbed case.

D. CASE 3

For Case 3, the soliton is placed at 80 km from the source. A plot of the acoustic arrival structure for this case is shown in Figure 16. The first, second, and sixth arrivals have a sound pressure than the unperturbed case. The fourth arrival for case 3 has a higher sound pressure than the unperturbed case.

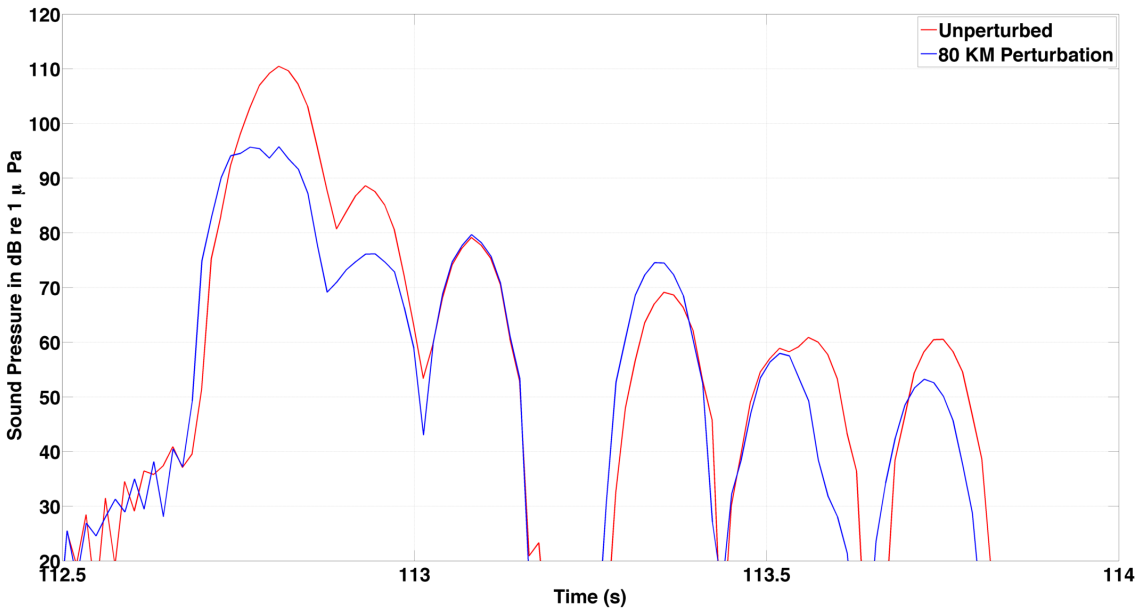

Figure 16. Acoustic arrival structure (receive level versus travel time) for case 3 (blue) and for the unperturbed case (red).

The eigenrays for the first, second, fourth, and sixth arrivals for Case 3 are shown in Figure 17. Case 3 is in blue and the unperturbed case is in red. The first arrival is lower due to that the eigenrays have additional bottom interactions. For the second arrival there are two eigenrays for Case 3 and the unperturbed case. The two rays are more out of phase for Case 3 than the unperturbed case. The sixth arrival for case 3 contains only 8 eigenrays, while the unperturbed case contains 15 rays.

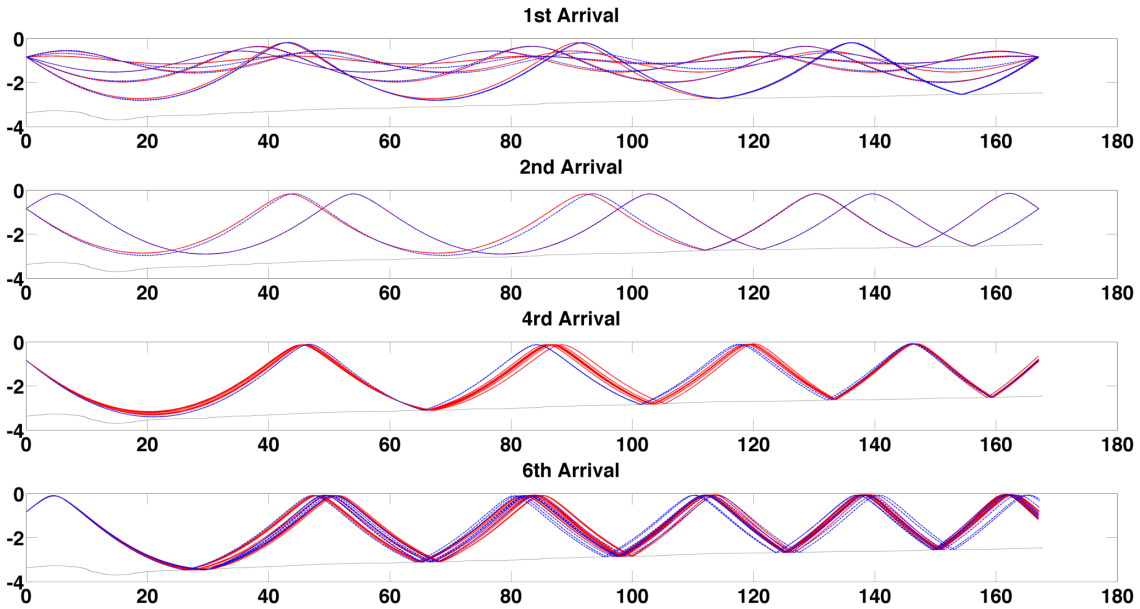

Figure 17. The eigenrays for the 1st, 2nd, 4th, and 6th arrivals for Case 3 (blue) and for the unperturbed case (red).

A plot of the number of bottom bounces versus initial launch angle is shown in Figure 18. Several of the eigenrays for the first arrival of Case 3 have additional bottom interactions. This increased bottom interaction lead to increased bottom loss for the first arrival of Case 3. A plot of bottom loss versus initial launch angle is shown in Figure 19. The increased bottom loss is highlighted with a black circle in Figure 19.

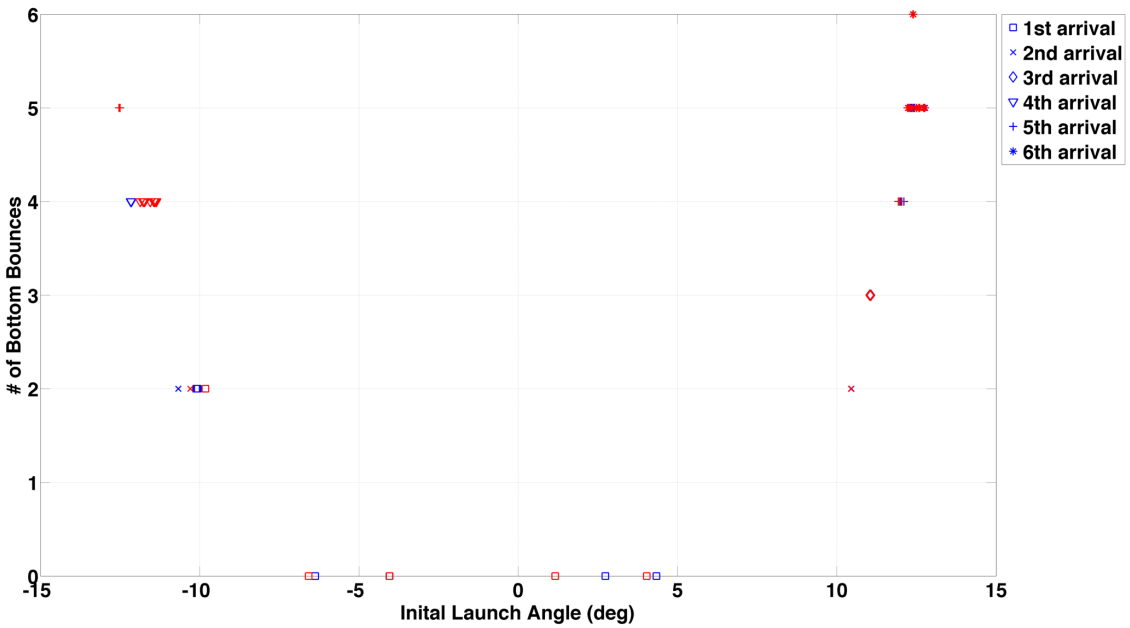

Figure 18. Number of bottom bounces versus initial launch angle for Case 3 (blue) and for the unperturbed case (red).

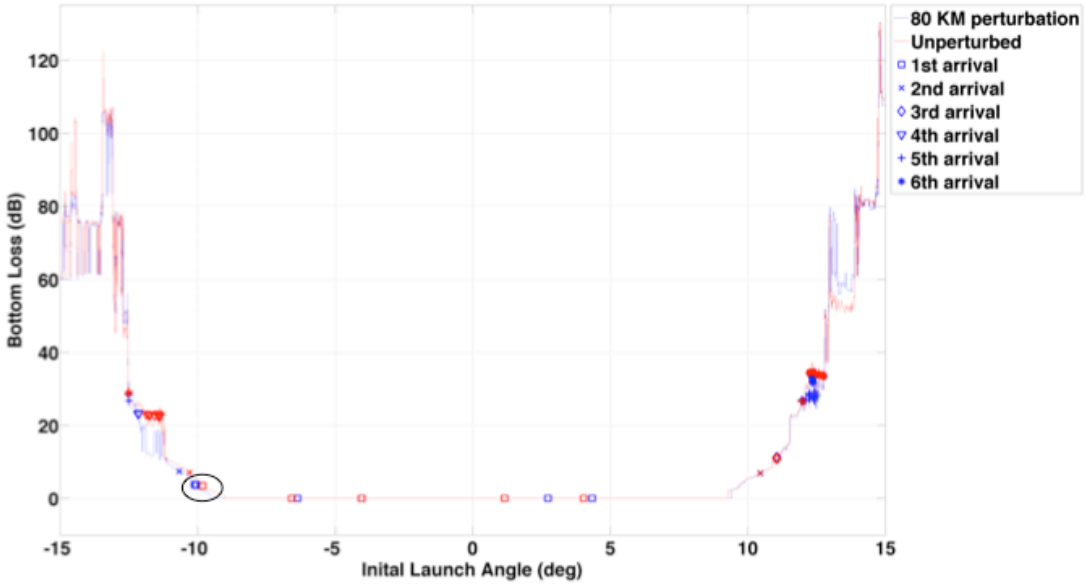

Figure 19. Bottom loss versus initial launch angle (solid lines) for Case 3 (blue) and for the unperturbed case (red). Discrete symbols denote eigenrays. Black circles highlight the higher bottom loss for the 1st arrival of Case 3.

The fourth arrival for Case 3 has less bottom loss than the unperturbed case. This is highlighted with a black circle in Figure 20. This change is due to the change of the ray angle at bottom for these rays. The eigenrays for the fourth arrival are represented as triangles.

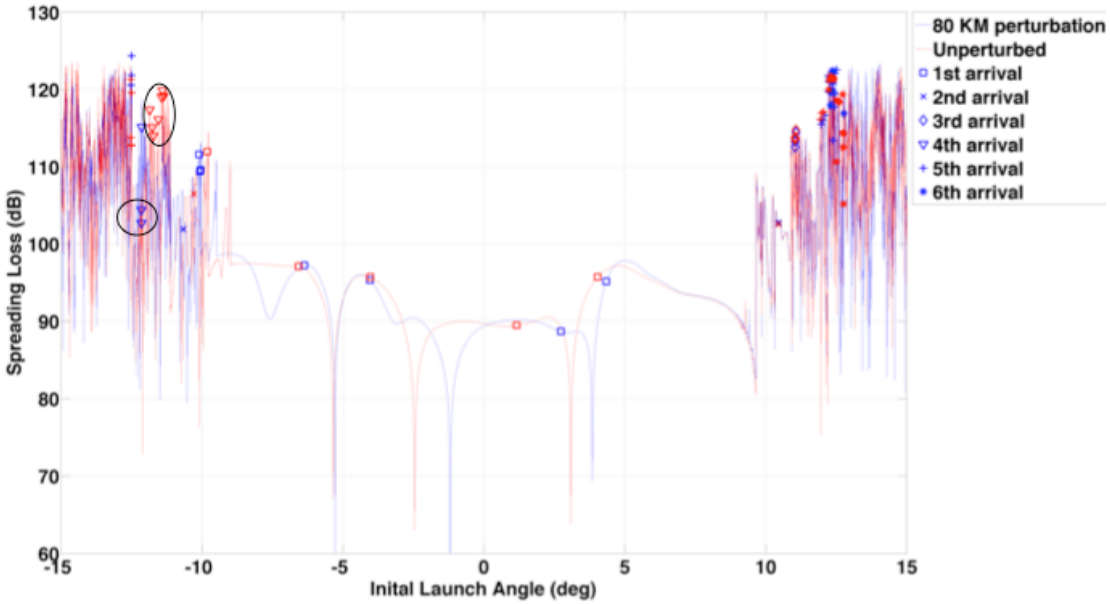

Figure 20. Ray tube-spreading loss versus initial launch angle (solid lines) for Case 3 (blue) and for the unperturbed case (red). Discrete symbols denote eigenrays. Black circle highlight the difference in spreading loss for the 4th arrival.

E. CASE 4

For case 4, the introduction of a soliton did not significantly change the arrival structure. In case 4, the soliton is placed at 120 km from the source. A plot of the acoustic arrival structure for this case is shown in Figure 21. The eigenrays for case 4 follow a very similar path to the eigenrays of the unperturbed case. A plot of the eigenrays for all of the arrivals in case 4 is shown in Figure 22.

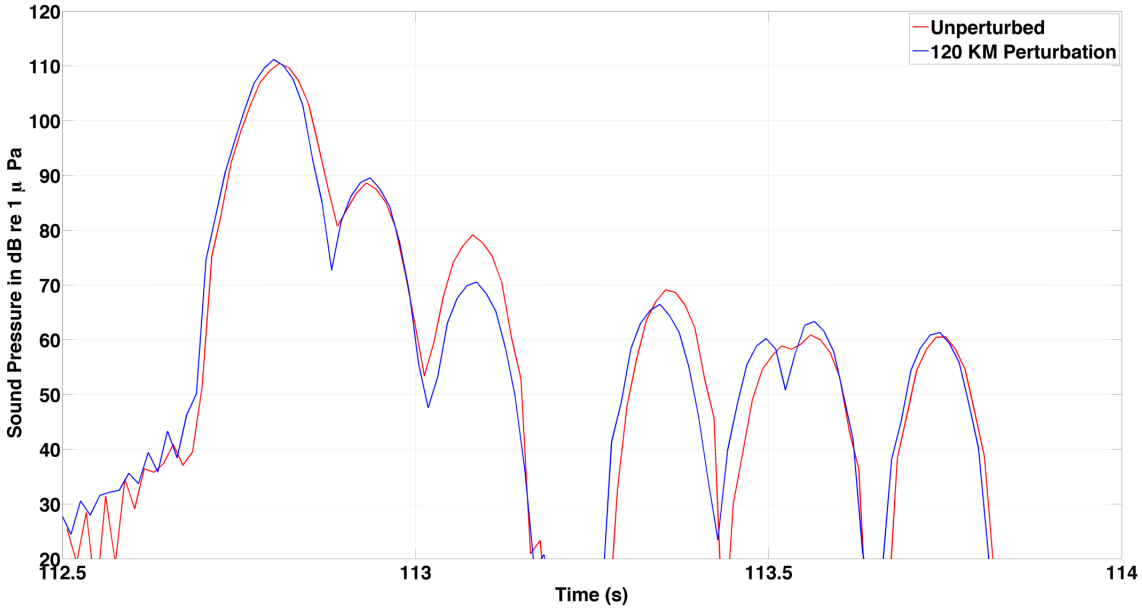

Figure 21. Acoustic arrival structure (receive level versus travel time) for Case 4 (blue) and for the unperturbed case (red).

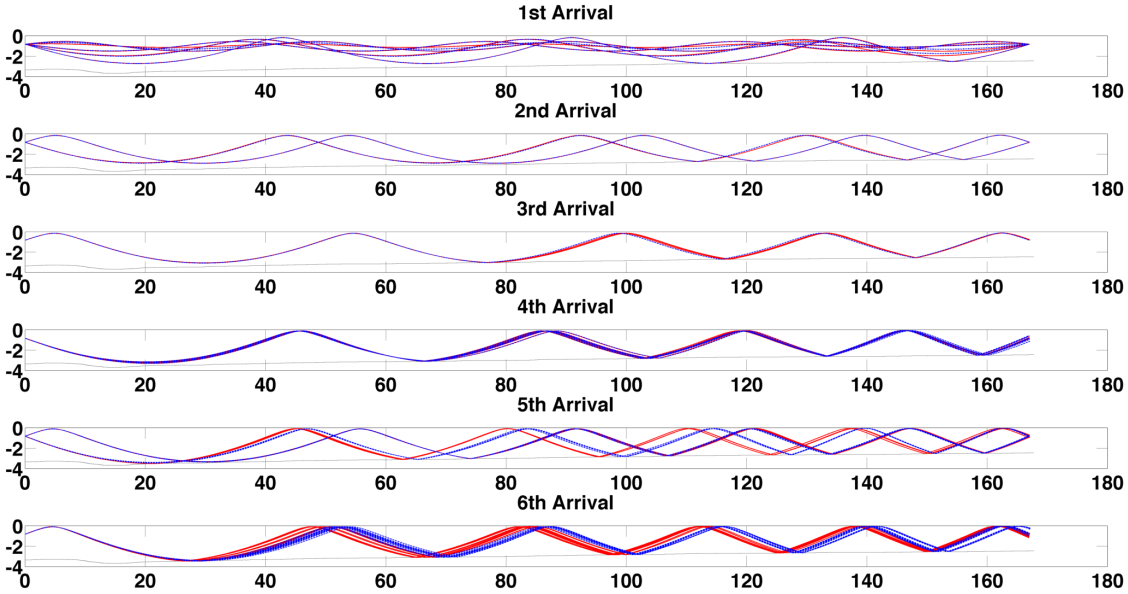

Figure 22. The eigenrays for all arrivals for Case 4 (blue) and for unperturbed case (red).

F. CASE 5

For Case 5, the soliton is placed at 160 km from the source. A plot of the acoustic arrival structure for this case is shown in Figure 23. The arrival structure for Case 5 is very similar to the unperturbed case. The soliton has very little effect on the eigenrays. A plot of the eigenrays for all of the arrivals for Case 5 is shown in Figure 24.

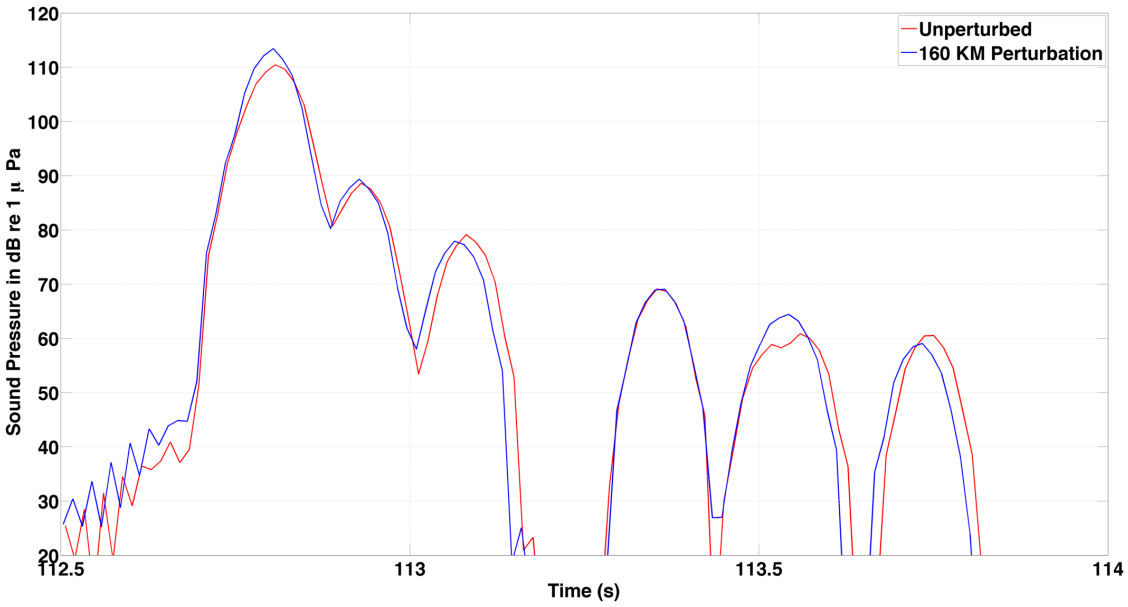

Figure 23. Acoustic arrival structure (receive level versus travel time) for Case 5 (blue) and for the unperturbed case (red).

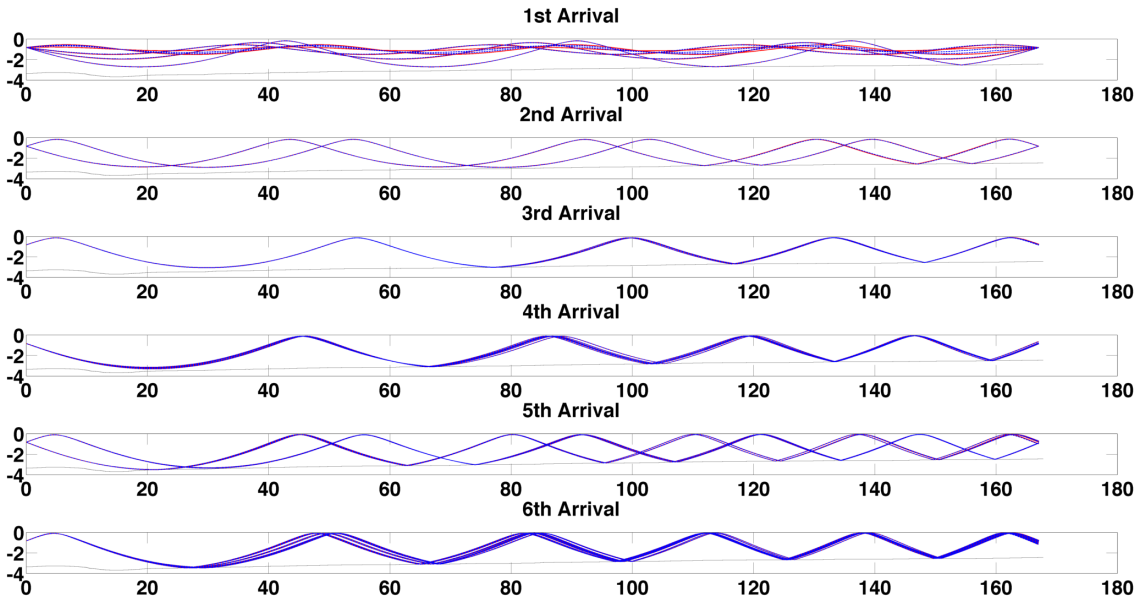

Figure 24. The eigenrays for all arrivals for Case 5 (blue) and for the unperturbed case (red).

IV. CONCLUSIONS

The objective of this research was to model and study the effects of the transbasin internal waves on low-frequency signal transmission through the SCS basin. Specifically, the fluctuations in the multipath arrival structure of a 400-Hz acoustic pulse transmitted through a distance of 167-km in the NE SCS basin in the presence an internal ocean soliton were studied. The approach of this thesis was to develop a numerical model of a 400 Hz signal transmission through the SCS in the presence of a trans-basin internal soliton and then examine and contrast the modeled arrival structures at the receiver. The model is based on ray theory, and entails the integration of a raytracing model and an eigenray ray search and arrival structure simulation code. The model permits the study of the physics and phenomenology of sound propagation though the SCS trans-basin nonlinear internal waves. A modeled range dependent sound speed profile, measured bathymetry and inferred bottom-loss characteristics from previous research were used.

Each perturbation case and the unperturbed case have six separate arrivals with robust travel time. However, large amplitude fluctuations were observed for each of these arrivals. The factors that affect the amplitude for each of the arrivals are changes in: the number of bottom interactions, ray tube spreading, phase interference and in the number of eigenrays making up an arrival. Micro-multipath arrivals affect a number of eigenrays for all arrivals. The results also show that the closer the soliton to the receiver, the less impact the soliton had on the arrival structure. This is because when the soliton was placed farther from the receiver, more bottom interactions downstream existed. Therefore changing the locations of these bottom interactions resulted in more changes in the arrival amplitude. As the range between the receiver and the soliton was decreased the perturbation had less effect on the location of bottom interactions and cause less change in the arrival structure.

Future research will entail a detailed model-data comparison of this model and the observations from the WISE experiment. This comparison will be both qualitative and quantitative in nature to further validate the model.

LIST OF REFERENCES

Bernotavicius, C. S., C. S. Chiu, C. W. Miller, D. B. Reeder, R. C. Wei, Y. J. Yang, and L. Chiu, 2010: Modeling a 400Hz signal transmission through the South China Sea basin. *J. Comp. Acous.* **18,** 193–208.

Chiu, C. S., S. R. Ramp, and C. Miller, 2004: Acoustic Intensity Fluctuations Induced by South China Sea Internal Tides and Solitons. *IEEE J. Ocean. Eng.*, **24,** 1249–1263.

Chiu, C. S., A. J. Semter, C. M. Ort, J. H. Miller, and L. L Ehert, 1994: A ray variability analysis of sound transmission from Heard Island to California. *J. Acoust. Soc. of Am.*,**96,** 2380–2388.

Department of Defense, cited 2013: Sustaining U.S.: Priorities for 21st century defense. [Available online at www.defense.gov/news/Defense_Strategic_Guidance.pdf]

Hager, C. A., 2008: Assessment of the Performance of the Near Bottom Hydrophones of the U.S. Navy southern California Offshore Range in Detecting, Localizing and Reconstructing 10–20 kHz Odontocete Whistles. Ph.D. dissertation, Naval Postgraduate School, 62 pp.

Hsu, M. K. and Liu A. K., 2000: Nonlinear internal waves in the South China Sea. *Can. J. Remote Sens.*, **26**, 72–81.

Liu, C. S., S. Y. Liu, S. E. Lallemand, N., Lundberg, and D. Reed, 1998: Digital elevation Model Offshore Taiwan and its Tectonic Implications. *Terrestrial, Atomspheric and Ocean Sciences 9*, **4,**750–753.

Medwin, H., and Coauthors, 2005; Ocean waveguides: scattering by rough surfaces, barriers, escarpments, and seamounts. *Sounds in the Sea: From Ocean Acoustics to Acoustical Oceanography,* Cambridge University Press, 233–267.

Medwin, H., 1975: Speed of Sound In Water: A Simple Equation for Realistic Parameters. *J. Acoust. Soc. of Am.*, **58,** 1318–1319.

Miller, C. W., M. Stone, K. Wyckoff, F. Bahr, 2009: The Windy Island and Soliton Experiment (WISE): Shallow Water and Basin Experiment Configuration and Preliminary Observations. NPS Technical Report, 103 pp.

Ramp, S. R., Y. J. Yang, F. L. Bahr, 2010: Characterizing the nonlinear internal wave climate in the northeastern South China Sea. *Nonlin. Processes Geophys.,* **17,** 481–498.

Wilks, D. S., 2006: Principle Component (EOF) Analysis. *Statistical Methods in the Atmospheric Sciences,* J. Hele, Academic Press, 463-507.

Ziomek, L. J., 1995: *Fundamentals of Acoustic Field Theory and Space Time Signal Processing.* CRC Press, 692 pp.

INITIAL DISTRIBUTION LIST

1. Defense Technical Information Center
   Ft. Belvoir, Virginia

2. Dudley Knox Library
   Naval Postgraduate School
   Monterey, California